TITLE:

Efficient room-temperature magnetization direction detection by means of the enhanced anomalous Nernst effect in a Weyl ferromagnet

AUTHOR(S):

Leiva, L.; Granville, S.; Zhang, Y.; Dushenko, S.; Shigematsu, E.; Ohshima, R.; Ando, Y.; Shiraishi, M.

京都大学学術情報リポジトリ
KURENAI 紅
Kyoto University Research Information Repository

Efficient room-temperature magnetization direction detection by means of the enhanced anomalous Nernst effect in a Weyl ferromagnet

L. Leiva [1], S. Granville [2,3], Y. Zhang [2,3], S. Dushenko,[1,4,5] E. Shigematsu,[1] R. Ohshima [1], Y. Ando [1], and M. Shiraishi[1]

[1]*Department of Electronic Science and Engineering, Kyoto University, Kyoto 615-8510, Japan*
[2]*Robinson Research Institute, Victoria University of Wellington, Wellington 6140, New Zealand*
[3]*The MacDiarmid Institute for Advanced Materials and Nanotechnology, Wellington 6011, New Zealand*
[4]*Institute for Research in Electronics and Applied Physics, University of Maryland, College Park, Maryland 20742, USA*
[5]*Physical Measurements Laboratory, National Institute of Standards and Technology, Gaithersburg, Maryland 20899, USA*

Spintronic phenomena exhibiting a longitudinal resistance change under magnetization reversal are a quite novel feature in nanoscience, which has been intensively studied in hopes of realizing all-electrical magnetization direction detection devices, where no reference ferromagnetic layer is required. However, cryogenic temperatures and/or high magnetic fields have been required to achieve noticeable effects. Here, the high heat-to-charge conversion efficiency of the Heusler alloy Weyl semimetal Co_2MnGa is exploited in single layer nanoscaled wires at room temperature to produce at least two orders of magnitude enhancement of the resistance change ratio, when compared with conventional ferromagnets. Such resistance change under magnetization reversal is consistently explained through temperature distribution simulations and direct thermoelectric measurements of the large anomalous Nernst effect (ANE) in this topologically nontrivial material. Although many reports consider ANE signals as perturbations or undesired artifacts, we demonstrate that they are dominant in this system and can be seized for nonvolatile memory readout, as shown in a prototype device. These results open up new horizons of using enhanced thermoelectric voltages in novel materials for magnetization direction detection in any system where significant temperature gradients exist.

I. INTRODUCTION

Recent progress in materials science is leading to the emergence of materials with increasingly high thermoelectric conversion efficiency [1]. Whilst most efforts have been concentrated in the conventional Seebeck effect, a variety of transport phenomena involving spin and heat have been discovered, giving birth to the field nowadays known as spin caloritronics [2–6]. In particular, magnetic materials exhibit the so-called anomalous Nernst effect (ANE), consisting in the generation of an electric field perpendicular to both an existing temperature gradient ∇T and the magnetization M, following the expression [6]

$$E_{ANE} = Q_s(\mu_0 M \times \nabla T) = S_{xy}\hat{m} \times \nabla T, \quad (1)$$

where Q_s is the anomalous Nernst coefficient, μ_0 is the vacuum permeability, S_{xy} is the anomalous Nernst thermopower, and $\hat{m}$ is a unit vector in the magnetization direction. Very recently, such effect was proven to be particularly strong in the topological materials known as Weyl ferromagnets [7], where the large ANE is thought to be originated from the sizable Berry curvature distribution around the Fermi level, associated with nodal lines or Weyl points [8]. In particular, ferromagnetic full Heusler compound Co_2MnGa has shown the largest room-temperature value for S_{xy} known to date, which is around 6.0 $\mu V/K$ [9,10] in bulk single crystals and between 2.0 and 6.0 $\mu V/K$ in thin films [11–13]. This joins

a variety of interesting properties of Co_2MnGa, such as a large anomalous Hall angle [14], large spin Hall angle [15], and a high resistance to oxidation [16], which pose it as a very promising material in the field of spintronics and spin caloritronics. In addition, it is also known that the transverse thermopower can be significantly enhanced by combining a Seebeck effect current and the anomalous Hall effect (AHE) in hybrid structures [17].

On the other hand, over the past decade it has been proved that spin torques originated by the spin-orbit interaction (a relativistic effect in solids) allow the magnetization switching of a ferromagnetic layer, the main mechanisms to accomplish it being the Rashba interaction and the spin Hall effect (SHE), which are electric current driven and do not require a fixed reference ferromagnet (FM) [18–20]. Such systems provide a technique to write a ferromagnetic memory element, but the counterpart reading scheme, i.e., a method to detect 180° magnetization reversal by purely electrical means in a practical scale, remains a challenge for physics [21]. To note is that the most well-known effect of the magnetization in the conductivity of a ferromagnet, the anisotropic magnetoresistance (AMR) [22], exhibits a 180°-periodic angular dependence on the magnetization direction and, therefore, cannot be used to distinguish between opposite magnetizations directions unless an external field that breaks such symmetry is applied [23]. The same constraint applies to the more recently discovered spin Hall magnetoresistance (SMR), due to its 180°

magnetization angle periodicity [24]. Thus AMR and SMR are not suitable for memory elements.

However, a few novel phenomena have shown a 360° periodicity in the magnetization angle dependence of the longitudinal resistance [21,25–28], which allows for discerning the magnetization direction of a single ferromagnetic layer by means of a straightforward resistance measurement. Therefore, utilization of such effects facilitates novel spintronic devices with simplified structures, such as a two-terminal geometry for magnetization direction readout. From now on, in this paper we will use the terminology unidirectional magnetoresistance (UMR) in a general way to refer, from a phenomenological point of view, to any electrical signal in longitudinal geometry (parallel to current) which is odd under magnetization reversal. In order to compare between different systems, a measure of the magnitude of the UMR is given by the relative change of the resistance, which we call UMR ratio and can be defined as $|R_P - R_{AP}|/R_{\mathrm{ave}}$, where R_P and R_{AP} refer to the resistance measured for parallel and antiparallel projections of the magnetization along some convenient axis, respectively, and R_{ave} is their average. UMR can manifest in bilayer FM/normal metal systems as an interface effect named unidirectional spin Hall magnetoresistance (USMR) [25], but as well it has been reported in magnetic/nonmagnetic semiconductor bilayers [21], FM/topological insulator (TI) bilayers [26], and magnetic/nonmagnetic TI bilayers [27,28]. It is also known that UMR can be Rashba-field mediated, as reported for systems such as two-dimensional electron gases [29,30] and Ge(111) [31], where the resistance change under magnetic field reversal is considered, since there is no magnetic order. However, some combination of cryogenic temperature requirements, use of high magnetic fields, and small UMR ratio at room temperature hinders any practical application of these phenomena.

Here in this study, with the aim of overcoming such limitations, we have focused on enhanced spin-caloritronic effects arising from topological properties in solids. In all of the aforementioned cases, the vertical asymmetry of a stacked film structure on top of a substrate, combined with Joule heating due to existent charge currents, favors the spontaneous generation of vertical thermal gradients [32,33]. Such temperature gradients may induce signals with UMR-like symmetry by means of the ANE or the combination of longitudinal spin Seebeck effect (LSSE) and inverse spin Hall effect (ISHE) [34]. Although these spin-caloritronic signals have been considered before [18,21,25,33,35], they were not dominant and many times just a small perturbation. In this work, we reveal that ANE-mediated UMR is dominant in Co$_2$MnGa thin wires, where the large ANE in this topological material and the device geometry were exploited to achieve at least two orders of magnitude enhancement with respect to both this same effect in conventional ferromagnets and any other report of UMR at room temperature.

II. RESULTS AND DISCUSSION

This section is organized into five subsections. In subsection A we study the symmetry of the resistance of Hall bar devices when performing angular scans of the applied external magnetic field in three perpendicular planes. From here, we identify and separate the signal responsible for the unidirectional effect. In the following subsection B, we focus on the electric current and magnetic field intensity dependence to obtain a behavior consistent with an ANE origin of the UMR effect. In subsection C we make a comparison with other conventional ferromagnetic materials to put in evidence that the observed UMR is much greater in Co$_2$MnGa than in other ferromagnets, which may be associated with the Weyl nature of Co$_2$MnGa. Then, in subsection D, we perform temperature distribution calculations together with thermopower measurements to corroborate that the magnitude of the UMR effect is consistent with an ANE origin. Finally, in subsection E, we propose a two-terminal device to distinguish magnetization direction from a simple resistance measurement.

A. Angular dependence of the magnetoresistance

The samples consisted of 30- to 50-nm-thick Co$_2$MnGa films epitaxially grown on a (001)-oriented MgO substrate. Then the films were patterned into sub-micron-scale Hall-bar-like devices using electron beam lithography (EBL) and argon ion milling techniques. The width W of these Hall bars varied from 100 nm to 400 nm, while their lengths L were varied in a way that the aspect ratio L/W was always kept on the order of 50, with the intention of comparing devices with similar resistance. Finally, 100-nm-thick Cu macroscopic connection pads were made by using EBL and thermal evaporation techniques, with an intermediate milling step in order to reduce interface resistances.

To study the dependence of the resistance on the direction of the magnetization of the ferromagnet, a conventional four-probe measurement was performed while applying an external magnetic field and varying the orientation of the sample with respect to such field. The geometry of the magnetic field angular scans is shown in Fig. 1(a). In all the cases, the external magnetic field was set at $B = 6$ T, which is large enough to assure that the magnetization of the sample is always parallel to the magnetic field, as shown in Sec. S1 of the Supplemental Material [36]. Both the longitudinal R_L and transverse R_T resistances were obtained, and they were decomposed into an even part $R_{L/T}^{\mathrm{even}} = [R_{L/T}(I_c) + R_{L/T}(-I_c)]/2$ and an odd part $R_{L/T}^{\mathrm{odd}} = [R_{L/T}(I_c) - R_{L/T}(-I_c)]/2$, on the basis of their response to an inversion of the injected dc charge current I_c. Since the Joule heating depends on the square of the current, the thermally originated signals are expected to manifest in the even part of the measured voltages V_L and V_T and, therefore, in the odd part of the resistances. This odd component was proven to be equivalent to the second harmonic resistance in a lock-in measurement, as shown in Sec. S2 of the Supplemental Material [36]. All the transport measurements were performed at room temperature unless otherwise stated.

Figures 1(b) and 1(c) show both the even and odd components of the longitudinal and transverse resistances, respectively, as functions of the magnetic field angle for scans performed within three perpendicular planes. The UMR behavior, attributed to the ANE in Co$_2$MnGa as discussed later, appeared in R_L^{odd} for the xy and zy scans, where the resistance shows a 360° periodicity. The extreme values correspond to angles of 90° and 270°, where the charge current and the
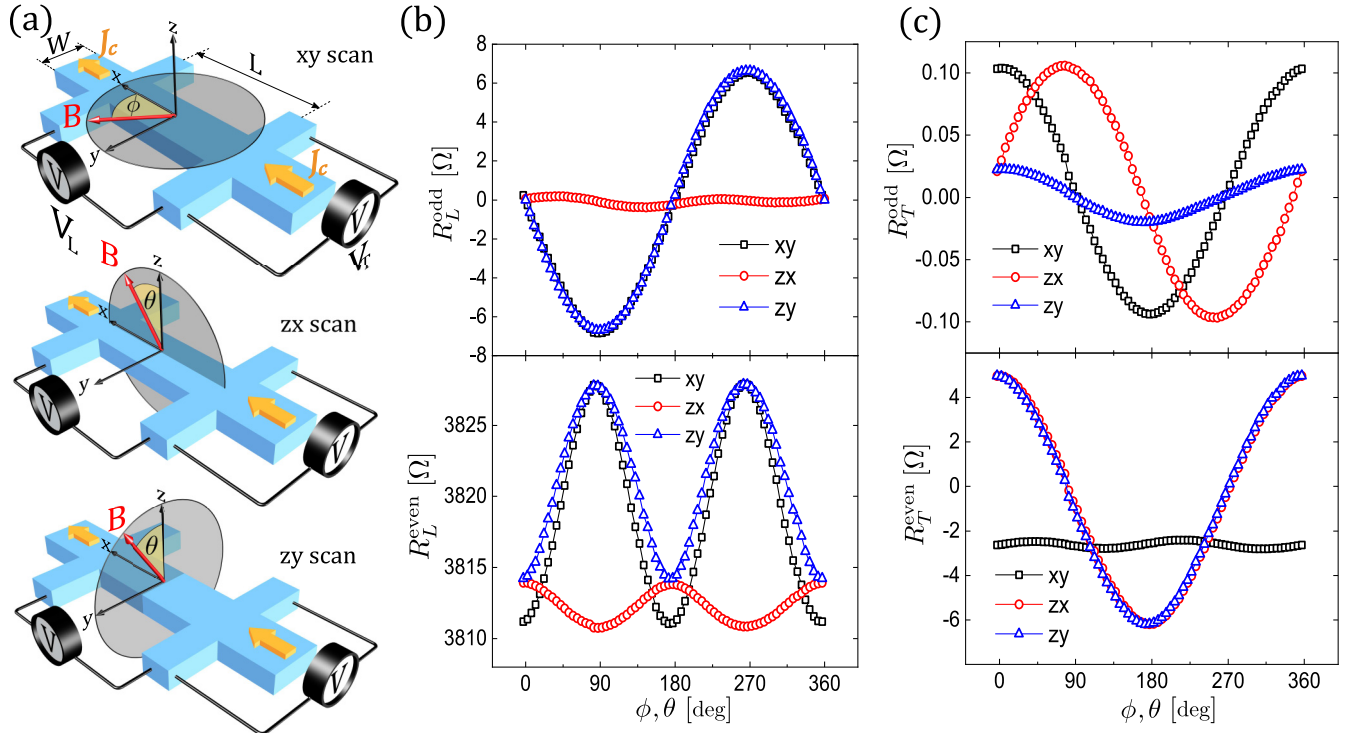
FIG. 1. (a) Schematics of Hall bar devices. The definition of axis, angle scans, dimensions, and electrical connections are shown. (b) Longitudinal resistance for three perpendicular magnetic field scans. The odd component (top panel) is governed by ANE voltages for *xy* and *zy* scans, while the even component (bottom panel) is governed by AMR phenomena. (c) Transverse resistance for three perpendicular magnetic field scans. The odd component (top panel) is again dominated by ANE voltages, while the even component (bottom panel) is ruled by the AHE for *xy* and *zy* scans.

magnetization are perpendicular to each other. A 360° periodicity was observed as well in the transverse odd component R_T^{odd} for the *xy* and *zx* scans, where the resistance reaches an extreme value when the magnetization and the charge current are either parallel or antiparallel to each other, contrary to the R_L^{odd} case. This can be understood as the transverse projection of the ANE-originated electric field, which is consistent with the observed magnitudes given that the quotient between longitudinal and transverse odd resistance amplitudes was found to be around the aspect ratio of the Hall bars. Concerning the even components, R_L^{even} is dominated by AMR phenomena, where a characteristic negative AMR was observed, as previously reported [37]. On the other hand, R_T^{even} is governed by the strong AHE in Co$_2$MnGa, where the anomalous Hall angle was found to be around 9%, which is consistent with previous studies [14,15]. More detail on the decomposition and identification of the resistance signals based on their symmetry can be found in Sec. S3 of the Supplemental Material [36].

B. Current density and magnetic field dependence of the magnetoresistance

The schematics of Fig. 2(a) show the vertical gradient produced by Joule heating due to a charge current on a piece of ferromagnetic wire. When the in-plane magnetization is perpendicular to such gradient, an ANE-originated electric field E_{ANE} will be generated parallel to the current density J_C^+, and therefore parallel to the electric field E_C^+ following Ohm's law. As shown in the figure, E_{ANE} can be understood, in a

macroscopic picture, as the result of electrons being scattered into a preferential direction. Since the thermal gradient is expected to be the same for positive or negative current, E_{ANE} will not change when the current is inverted into J_C^- and, therefore, the total electric fields E_L^+ and E_L^- will differ in absolute value.

Figure 2(b) shows the longitudinal resistance for positive and negative currents in an *xy* scan of the external magnetic field for a current density of 2.75×10^{11} A/m^2, being remarkable that the UMR contribution is as significant as the conventional AMR. The current density dependence of the odd component of the longitudinal resistance was found to be linear, as shown in Figs. 2(c) and 2(d), where the UMR ratio is defined, for an *xy* scan, as

$$\text{UMR ratio} = \frac{R_L^{\text{odd}}(\phi = 270°) - R_L^{\text{odd}}(\phi = 90°)}{R_L^{\text{even}}(\phi = 90°)}. \quad (2)$$

If Joule heating due to the injected current is considered to be the only source of the thermal gradient, it is reasonable to assume $\nabla T \propto I_c^2 R_s$, where R_s is the sample resistance. Then, the ANE voltage V_{ANE} will be quadratic in current and, therefore, the resistance $R_{\text{ANE}} = V_{\text{ANE}}/I_c$ will be linear in current. Although such linear behavior is clear for low current densities, a saturation of the UMR ratio was systematically observed above about 2.5×10^{11} A/m^2, as shown in Fig. 2(d). This saturation, however, is not due to an irreversible deterioration of the device, since the linear regime is recovered when the current density is decreased.
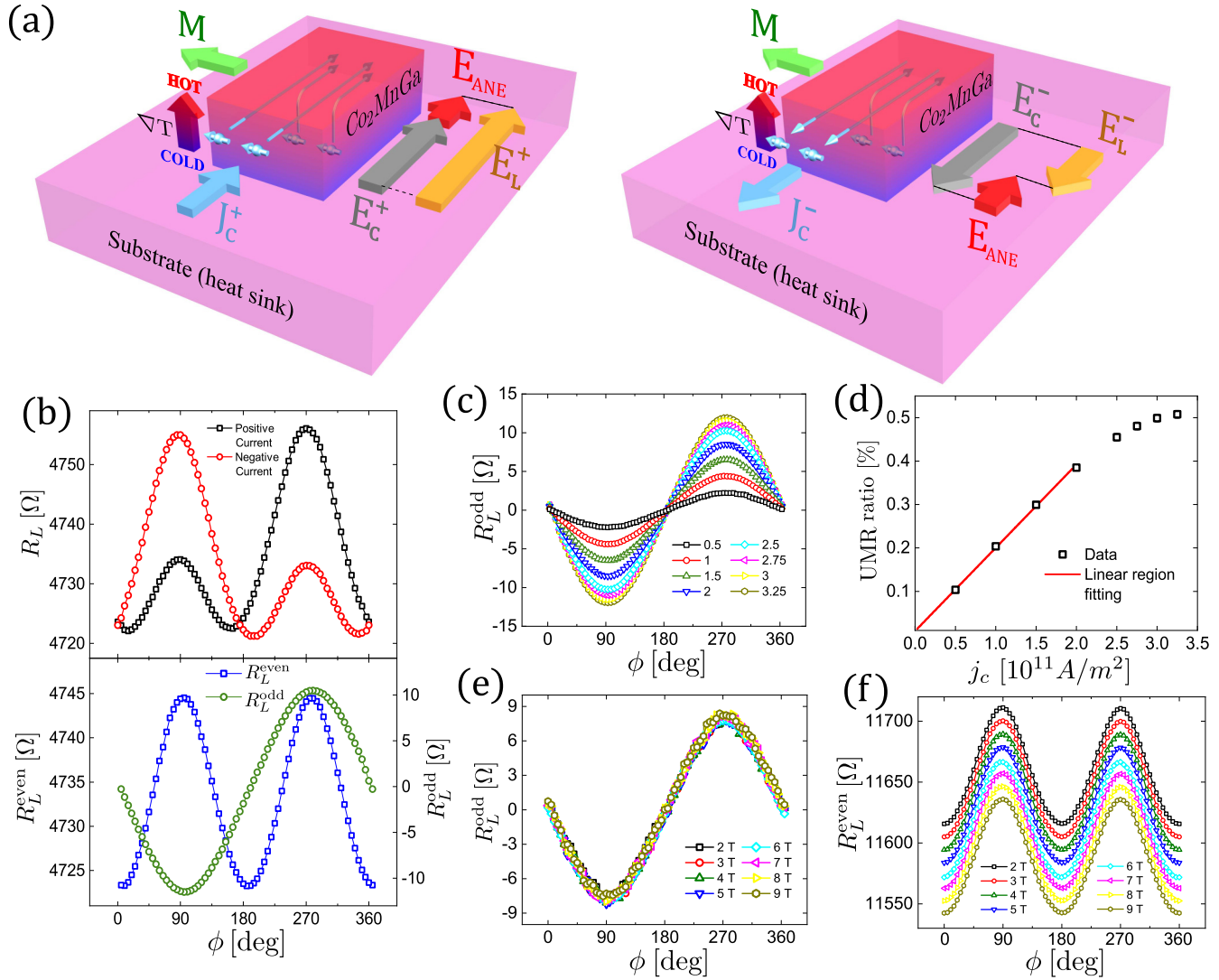
FIG. 2. (a) Schematics of a piece of Co₂MnGa wire on top of an MgO substrate, where a charge current J_C^+ or J_C^- produces a thermal gradient due to Joule heating and the asymmetric boundary conditions. The ANE-generated electric field E_{ANE}, which is independent of the direction of the electric current, produces an asymmetry in the total electric fields for each current direction E_L^+ and E_L^-, giving rise to the UMR effect. (b) Example of the longitudinal resistance measured for an *xy* scan of magnetic field angle, for a current density of 2.75×10^{11} A/m². The top panel shows the resistance measured for positive and negatives currents, while the bottom panel shows even and odd components. (c) Odd component of longitudinal resistance for an *xy* scan for several current densities, in units of 10^{11} A/m². (d) Current density dependence of the UMR ratio. (e),(f) Magnetic field intensity dependence of the odd (e) and even (f) components of the longitudinal resistance for an *xy* scan.

To obtain further compelling evidence that the ANE is the central origin of the UMR, the magnetic field intensity dependence is analyzed. Once the magnetization is saturated along a certain direction, further increase of the external magnetic field should produce no effect in V_{ANE} and consequently the odd part of the resistance should be independent of the magnetic field intensity, as shown in Fig. 2(e) for external magnetic fields from 2 T up to 9 T. The independence of the resistance from the magnitude of the magnetic field unequivocally excludes nonreciprocal charge transport that frequently takes place in systems with breaking of inversion symmetry [38]. On the other hand, a decrease of the even part of the resistance was observed when increasing the external magnetic field, as shown in Fig. 2(f). Although a nonsaturating negative longitudinal magnetoresistance is known to

be a characteristic of nonmagnetic Weyl semimetals [39], it should follow a particular anisotropy as a function of the angle between the electric field E and the magnetic field H (for example, it should be zero when $E \perp H$), which is not this case. However, an angle-independent negative magnetoresistance has already been reported for Co₂MnGa thin film systems in a wide temperature range [14,40], where the authors attribute the effect to the suppression of thermal spin-dependent scattering.

C. Size and material influence in the UMR ratio

Further enhancement of the room-temperature UMR ratio was achieved when reducing the width of the nano-scale wires, as shown in Fig. 3(a). This trend is a very promising
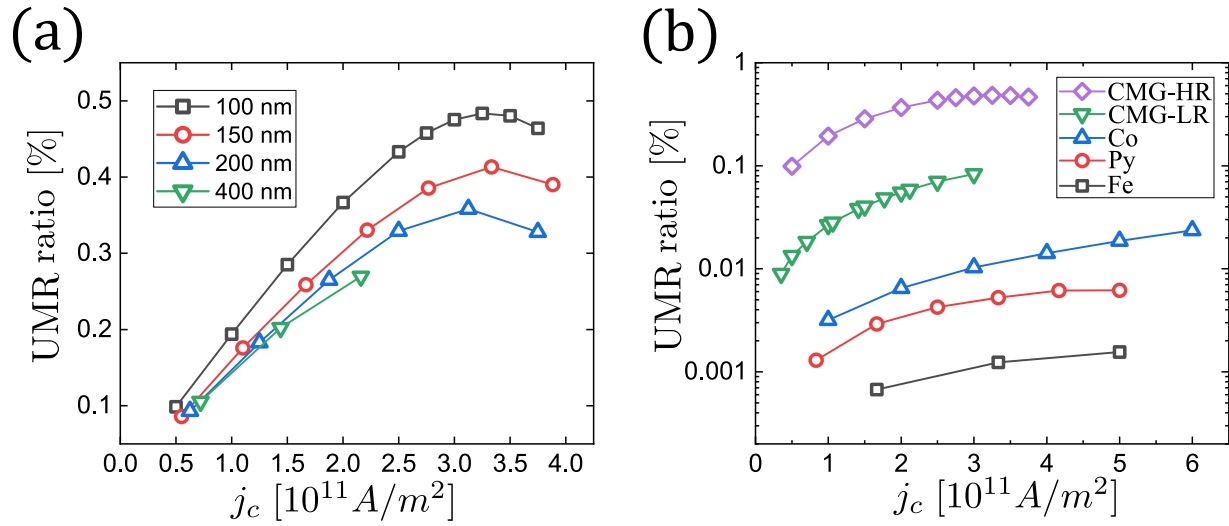
FIG. 3. (a) Current density dependence of the UMR ratio measured for different widths of Co₂MnGa Hall bars. (b) Current dependence of the UMR ratio measured for 200-nm-width and 30-nm-thick Hall bars made of different ferromagnetic materials, including low resistivity and high resistivity Co₂MnGa samples.

feature from an application point of view, given the efforts put in modern electronics towards the development of increasingly compact devices. It was observed as well that the saturation current density, that is, when the linear dependence is lost, also systematically increases for narrower wires. A room-temperature UMR ratio of up to 0.5% was observed for a 100-nm-width Hall bar.

A material comparison helps in understanding the significance of the topological nature of Weyl ferromagnets in the UMR. Figure 3(b) shows UMR ratios of a wide variety of ferromagnetic materials as a function of electric current density. All the compared samples were 200 nm width and 30 nm thick, plus a 2-nm-thick MgO capping layer in the case of Co, Fe, and Permalloy (Py). Two Co₂MnGa samples with very different resistivities were compared as well. Even though the crystalline $L2_1$ structure was verified in both cases (see Sec. S4 of the Supplemental Material [36]), the sample *CMG-HR* exhibited a resistivity as high as 210 $\mu\Omega$ cm, while sample *CMG-LR* resistivity was 113 $\mu\Omega$ cm. This difference is thought to be due to the use of targets from different manufacturers and different growth conditions such as the Ar pressure during sputtering [13]. Although both the heating (thought to be responsible for the UMR effect) and the resistance itself are proportional to the resistivity, which would lead to the same UMR ratio since they cancel each other, a surprising roughly tenfold increase was observed for the high resistivity sample, as shown in Fig. 3(b). Such increase is thought to be originated from a decrease of the thermal conductivity when the resistivity increases, resulting in a larger temperature gradient across the wire thickness. This is supported by the fact that, in metals, a significant contribution k_e to the total thermal conductivity k_t is given by the heat

transport through electrons, which shares mechanisms with the electron transport. From this basis, it can be derived that k_e has a linear relation with the electrical conductivity, as stated by the Wiedemann-Franz law [41]. A surprising roughly 100-fold increase of the UMR ratio is observed in the *CMG-HR* sample compared with Py or Co and a 500-fold increase when compared with Fe.

D. Temperature gradient computation and thermopower measurements

To obtain further supporting evidence that the odd component of the resistance is fully explained in terms of ANE-originated voltages, the vertical temperature gradient inside the ferromagnetic wire has to be estimated. Since the experimental determination of a thermal gradient across a distance as short as 30 nm is extremely difficult, a series of numerical multiphysics simulations were performed to compute the temperature distribution in the system, introducing Joule heating as the heat source. More details on these simulations, including a list of the involved parameters and their influence in the final result, is available in Sec. S5 of the Supplemental Material [36]. An example of the temperature distribution when the boundary condition is a fixed injection current of 1.5×10^{11} A/m² is shown in Fig. 4(a). Since the temperature gradient is not necessarily uniform along the wire thickness t, the generated E_{ANE} will depend on z, and a spatial average in this coordinate $\langle E_{\text{ANE}} \rangle$ must be considered when calculating the voltage. When the magnetization of the ferromagnet is along y direction, and assuming $\nabla\boldsymbol{T}$ is roughly uniform along the width of the wire, V_{ANE} can be written using Eq. (1) as

$$V_{\text{ANE}} = \langle E_{\text{ANE}} \rangle L = \frac{L}{t}\int_{-t}^{0} S_{xy}\nabla T\, dz = \frac{LS_{xy}(T_T - T_B)}{t} = \frac{LS_{xy}\Delta T}{t},\tag{3}$$
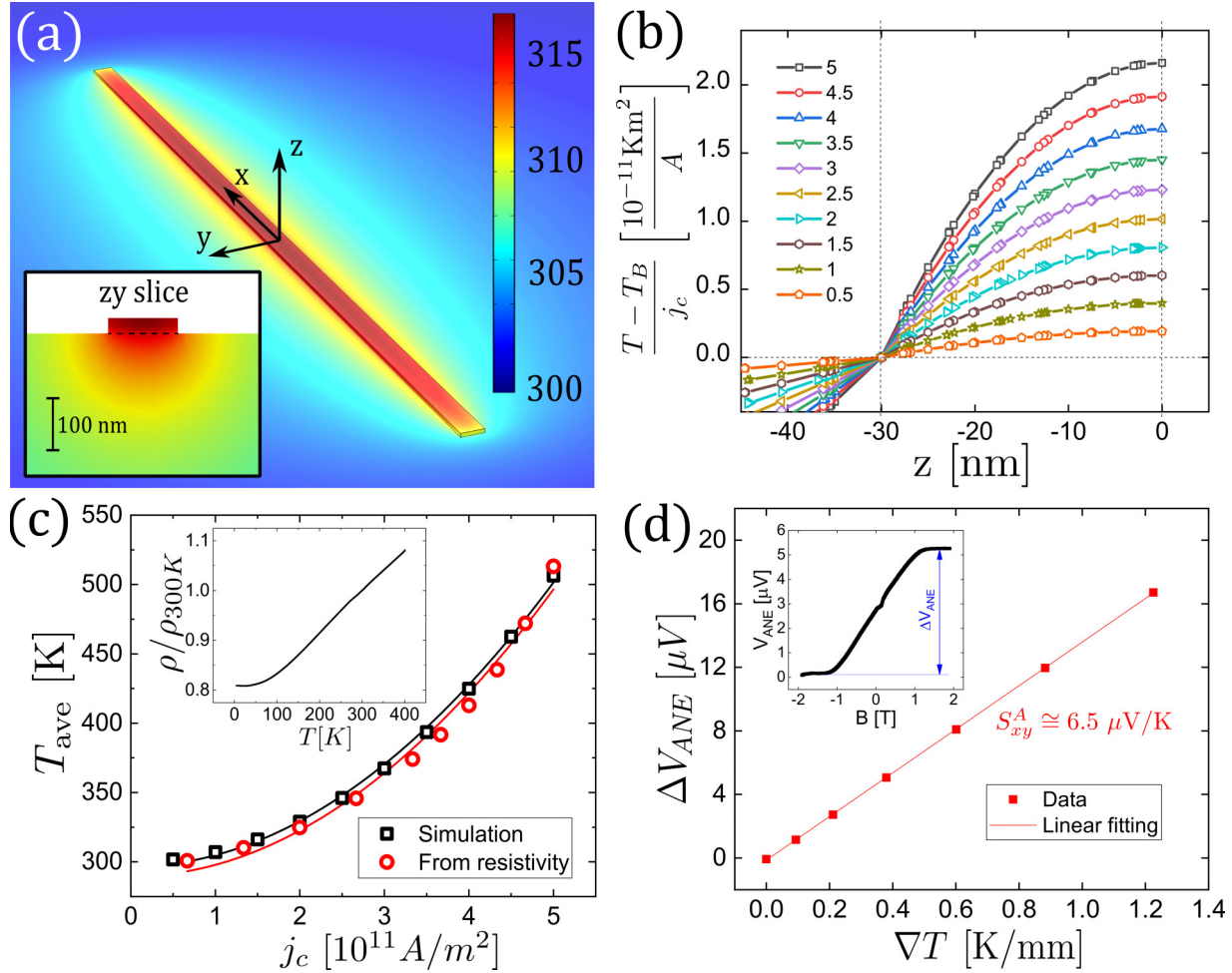
FIG. 4. (a) Simulated temperature spatial distribution, for a current density of 1.5×10^{11} A/m^2 along x direction. (b) Simulated temperature difference with respect to the bottom of the wire ($z = -30$ nm), normalized by current density, as a function of the distance along a vertical axis through the middle of the wire. Different plots correspond to different current densities, in units of 10^{11} A/m^2. (c) Current density dependence of the average temperature of the wire. Both simulation and estimation from resistivity measurements are shown, with the corresponding quadratic fittings in solid line. The inset shows the temperature dependence of the normalized resistivity. (d) Temperature gradient dependence of the ANE signal, which is obtained, as shown in the inset, by subtracting the saturation ANE voltages for positive and negative external magnetic fields.

where $T_T = T(z = 0$ nm$)$ and $T_B = T(z = -30$ nm$)$ are the temperatures at the top and the bottom of the wire, respectively. Therefore, V_{ANE} depends only on the temperature difference between top and bottom of the wire and not the distribution inside. The temperature profiles along z direction for several current densities, normalized by such current density, are shown in Fig. 4(b). The evenly spaced curves at $z = 0$ nm are consistent with the expected quadratic-in-current behavior of ∇T.

Although the temperature gradient cannot be directly measured, the average temperature of the wire T_{ave} can be estimated quite directly from the resistivity ρ. The inset of Fig. 4(c) shows a roughly linear dependence of the resistivity on the temperature in the region from 200 K up to 400 K, following the expression $\rho = \rho_{300\,\text{K}}[1 + \alpha(T - 300\,\text{K})]$, where $\rho_{300\,\text{K}}$ is the reference resistivity at 300 K. The resistivity temperature coefficient α was found to be 8×10^{-4} K^{-1}. This allowed us to adjust the simulation parameters, mainly

the substrate thermal conductivity, until the measured wire temperature and the calculated one were coincident, as shown in Fig. 4(c). To note is that temperatures as high as 500 K were achieved with current densities of 5×10^{11} A/m^2. Since the Curie temperature of Co$_2$MnGa has been reported as 687 K [42] and 694 K [43], it is possible that the loss of linearity in the UMR ratio for high current densities is related with a deterioration of the magnetic order.

The simulated ΔT values were in the order of a few kelvin, which over a thickness of 30 nm led to average temperature gradients in the order of 10^7 to 10^8 K/m. Knowing that E_{ANE} can be obtained in terms of R_L^{odd} from $E_{\text{ANE}} = R_L^{\text{odd}} I_c / L$, the required transverse thermopower to explain the value of E_{ANE} given the simulated temperature differences were in the same order of magnitude of the experimental reports of S_{xy}, although a little larger as shown in Table I. In addition, a direct measurement of the anomalous transverse thermopower of the Co$_2$MnGa high-resistivity thin films

TABLE I. Summary of the measured electric field and the temperature simulation results at several current densities for a 150-nm-wide and 30-nm-thick Co_2MnGa wire.

j_c (10^{11} A/m^2)	E_{ANE} (V/m)	Required ΔT (if $S_{xy} = 6\ \mu$V/K)	Simulated ΔT (K)	Required S_{xy} (μV/K)
0.73	64.7	0.32	0.23	8.41
1.46	267	1.33	0.92	8.68
2.22	604	3.02	2.11	8.55
2.95	1045	5.22	3.74	8.36
3.68	1563	7.81	5.84	8.02
4.44	2094	10.5	8.47	7.41
5.17	2419	12.1	11.5	6.3

employed in this work was performed by using a homemade sample holder designed to apply controlled in-plane thermal gradients (for more details on the experiment setup, check Sec. S6 of the Supplemental Material [36]). The results of the ANE voltage as a function of the temperature gradient are shown in Fig. 4(d), where the linear fitting leads to an S_{xy} of $-6.5\ \mu$V/K, which is similar to the maximum values previously reported in thin films and also quite consistent with the required S_{xy} according to the simulations. Consequently, attributing the measured UMR to solely the ANE contribution fits reasonably with all the observations.

E. Nonvolatile all-electrical two-terminal magnetization direction readout demonstration

As an experimental device demonstration utilizing the large UMR found in this study, a two-terminal memory read-out device was fabricated. To achieve this with no external magnetic field, the electrode remanent magnetization should be perpendicular to the injected current. Although an in-plane magnetocrystalline anisotropy exists (see Sec. S1 of the Supplemental Material [36]), it is much weaker than the shape anisotropy in prolate structures such as narrow thin wires. Therefore, the remanent magnetization direction can be forced by manipulating the electrode shape. As shown in Fig. 5(a), ferromagnetic electrodes of 16 μm width and

800 nm length were patterned. To test the influence of the crystalline direction of the electric current on the UMR, wires rotated 45° to each other were fabricated. 0° devices (left) were parallel to the [1$\bar{1}$0] crystalline axis, while 45° devices (right) are parallel to the [100] axis (see Sec. S4 of the Supplemental Material [36]). The odd component of the resistance was measured while sweeping the magnetic field in the directions shown in Fig. 5(a), obtaining the hysteresis curves shown in Fig. 5(b). Distinct high and low resistance states can be identified at zero magnetic field, corresponding to opposite directions of the remanent magnetization. However, no significant difference between 0° and 45° devices was observed, suggesting the generated E_{ANE} perpendicular to these two directions is the same. The most likely reason for this is that the temperature gradient direction is the same (out of plane) in both cases. Linear dependence of the UMR ratio on the current density was reproduced, with an earlier saturation than in narrower devices, following the trend of Fig. 3(b).

III. CONCLUSION

In conclusion, colossal enhancement of the relative change of the resistance under magnetization reversal was observed at room temperature in nanoscale wires of ferromagnetic Weyl semimetal Heusler alloy Co_2MnGa, when compared with
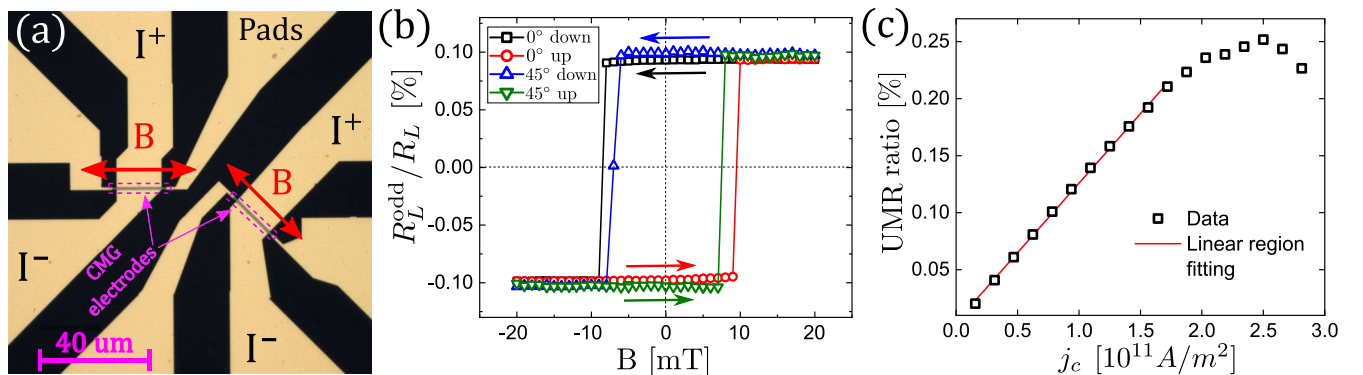

FIG. 5. (a) Microscope image of two-terminal devices showing electrical connections and magnetic field directions. The yellow areas are the connection pads made of gold and the thin gray strips are Co_2MnGa electrodes. Since this is tested in a two-terminal configuration, the pads where the current is applied (I^+, I^-) are the same pads used to measure the longitudinal voltage. There are also pads for a transversal voltage measurement, which are not used in this demonstration. (b) Odd component of the resistance, relative to total resistance, as a function of the external magnetic field, for 0° and 45° devices, for a current density of 1.5×10^{11} A/m^2. (c) Current density dependence of the UMR ratio measured for a 0° two-terminal device at room temperature.

control samples made of conventional ferromagnets. The analysis of the symmetry of the resistance with respect to rotations of the external magnetic field, together with current density and magnetic field intensity dependences, strongly suggest that the origin of such a significant magnetization-dependent voltage is entirely the combination of a spontaneous vertical thermal gradient and the particularly strong ANE in Co_2MnGa. It was observed as well that a higher resistivity or a narrower wire increase the aforementioned relative resistance change under magnetization reversal. In addition, simulations of the temperature distribution due to Joule heating and direct measurements of the transverse thermopower were consistent with both the observed electric fields and previous reports on the transverse thermopower of this material. These results show that the spin-dependent thermoelectric phenomena in magnetic materials can be thought not only for energy harvesting but as well for efficient room-temperature all-electrical two-terminal magnetization direction detection devices. Furthermore, if materials science keeps developing increasingly efficient thermoelectric materials, magnetization readout could be achievable by taking advantage of residual heat flows in electronic components instead of producing forced thermal gradients using high current densities.

[1] J. Wei, L. Yang, Z. Ma, P. Song, M. Zhang, J. Ma, F. Yang, and X. Wang, Review of current high-ZT thermoelectric materials, J. Mater. Sci. **55**, 12642 (2020).

[2] G. E. Bauer, E. Saitoh, and B. J. Van Wees, Spin caloritronics, Nat. Mater. **11**, 391 (2012).

[3] M. Hatami, G. E. W. Bauer, Q. Zhang, and P. J. Kelly, Thermal Spin-Transfer Torque in Magnetoelectronic Devices, Phys. Rev. Lett. **99**, 066603 (2007).

[4] K. Uchida, S. Takahashi, K. Harii, J. Ieda, W. Koshibae, K. Ando, S. Maekawa, and E. Saitoh, Observation of the spin Seebeck effect, Nature (London) **455**, 778 (2008).

[5] J. Flipse, F. Bakker, A. Slachter, F. Dejene, and B. Van Wees, Direct observation of the spin-dependent Peltier effect, Nat. Nanotechnol. **7**, 166 (2012).

[6] M. Mizuguchi and S. Nakatsuji, Energy-harvesting materials based on the anomalous Nernst effect, Sci. Technol. Adv. Mat. **20**, 262 (2019).

[7] F. Caglieris, C. Wuttke, S. Sykora, V. Süss, C. Shekhar, C. Felser, B. Büchner, and C. Hess, Anomalous Nernst effect and field-induced Lifshitz transition in the Weyl semimetals TaP and TaAs, Phys. Rev. B **98**, 201107(R) (2018).

[8] A. Markou, D. Kriegner, J. Gayles, L. Zhang, Y.-C. Chen, B. Ernst, Y.-H. Lai, W. Schnelle, Y.-H. Chu, Y. Sun, and C. Felser, Thickness dependence of the anomalous Hall effect in thin films of the topological semimetal Co_2MnGa, Phys. Rev. B **100**, 054422 (2019).

[9] A. Sakai, Y. P. Mizuta, A. A. Nugroho, R. Sihombing, T. Koretsune, M.-T. Suzuki, N. Takemori, R. Ishii, D. Nishio-Hamane, and R. Arita, Giant anomalous Nernst effect and quantum-critical scaling in a ferromagnetic semimetal, Nat. Phys. **14**, 1119 (2018).

[10] S. N. Guin, K. Manna, J. Noky, S. J. Watzman, C. Fu, N. Kumar, W. Schnelle, C. Shekhar, Y. Sun, J. Gooth, and C. Felser, Anomalous Nernst effect beyond the magnetization scaling relation in the ferromagnetic Heusler compound Co_2MnGa, NPG Asia Mater. **11**, 16 (2019).

[11] J. Hu, Y. Zhang, B. Wei, S. Tu, S. Liu, D. Yu, J.-P. Ansermet, S. Granville, and H. Yu, Anomalous Nernst effect in Co_2MnGa thin films with perpendicular magnetic anisotropy, J. Magn. Magn. Mater. **500**, 166397 (2020).

[12] G.-H. Park, H. Reichlova, R. Schlitz, M. Lammel, A. Markou, P. Swekis, P. Ritzinger, D. Kriegner, J. Noky, J. Gayles, Y. Sun, C. Felser, K. Nielsch, S. T. B. Goennenwein, and A. Thomas, Thickness dependence of the anomalous Nernst effect and the Mott relation of Weyl semimetal Co_2MnGa thin films, Phys. Rev. B **101**, 060406(R) (2020).

[13] K. Sumida, Y. Sakuraba, K. Masuda, T. Kono, M. Kakoki, K. Goto, W. Zhou, K. Miyamoto, Y. Miura, T. Okuda, and A. Kimura, Spin-polarized Weyl cones and giant anomalous Nernst effect in ferromagnetic Heusler films, Commun. Mater. **1**, 89 (2020).

[14] Y. Zhang, Y. Yin, G. Dubuis, T. Butler, N. V. Medhekar, and S. Granville, Berry curvature origin of the thickness-dependent anomalous Hall effect in a ferromagnetic Weyl semimetal, npj Quantum Mater. **6**, 17 (2021).

[15] L. Leiva, S. Granville, Y. Zhang, S. Dushenko, E. Shigematsu, T. Shinjo, R. Ohshima, Y. Ando, and M. Shiraishi, Giant spin Hall angle in the Heusler alloy Weyl ferromagnet Co_2MnGa, Phys. Rev. B **103**, L041114 (2021).

[16] B. M. Ludbrook, B. J. Ruck, and S. Granville, Perpendicular magnetic anisotropy in Co_2MnGa and its anomalous Hall effect, Appl. Phys. Lett. **110**, 062408 (2017).

[17] W. Zhou, K. Yamamoto, A. Miura, R. Iguchi, Y. Miura, K.-i. Uchida, and Y. Sakuraba, Seebeck-driven transverse thermoelectric generation, Nat. Mater. **20**, 463 (2021).

[18] I. M. Miron, K. Garello, G. Gaudin, P.-J. Zermatten, M. V. Costache, S. Auffret, S. Bandiera, B. Rodmacq, A. Schuhl, and P. Gambardella, Perpendicular switching of a single ferromagnetic layer induced by in-plane current injection, Nature (London) **476**, 189 (2011).

[19] L. Liu, C.-F. Pai, Y. Li, H. W. Tseng, D. C. Ralph, and R. A. Buhrman, Spin-torque switching with the giant spin Hall effect of tantalum, Science **336**, 555 (2012).

[20] M. Aoki, E. Shigematsu, M. Matsushima, R. Ohshima, S. Honda, T. Shinjo, M. Shiraishi, and Y. Ando, In-plane spin-orbit torque magnetization switching and its detection using the spin rectification effect at subgigahertz frequencies, Phys. Rev. B **102**, 174442 (2020).

[21] K. Olejník, V. Novák, J. Wunderlich, and T. Jungwirth, Electrical detection of magnetization reversal without auxiliary magnets, Phys. Rev. B **91**, 180402(R) (2015).

[22] T. McGuire and R. Potter, Anisotropic magnetoresistance in ferromagnetic 3d alloys, IEEE Trans. Magn. **11**, 1018 (1975).

[23] J. Daughton, Magnetoresistive memory technology, Thin Solid Films **216**, 162 (1992).

[24] H. Nakayama, M. Althammer, Y.-T. Chen, K. Uchida, Y. Kajiwara, D. Kikuchi, T. Ohtani, S. Geprägs, M. Opel, S. Takahashi, R. Gross, G. E. W. Bauer, S. T. B. Goennenwein, and E. Saitoh, Spin Hall Magnetoresistance Induced by a Nonequilibrium Proximity Effect, Phys. Rev. Lett. **110**, 206601 (2013).

[25] C. O. Avci, K. Garello, A. Ghosh, M. Gabureac, S. F. Alvarado, and P. Gambardella, Unidirectional spin Hall magnetoresistance in ferromagnet/normal metal bilayers, Nat. Phys. **11**, 570 (2015).

[26] N. H. Duy Khang and P. N. Hai, Giant unidirectional spin Hall magnetoresistance in topological insulator ferromagnetic semiconductor heterostructures, J. Appl. Phys. **126**, 233903 (2019).

[27] K. Yasuda, A. Tsukazaki, R. Yoshimi, K. S. Takahashi, M. Kawasaki, and Y. Tokura, Large Unidirectional Magnetoresistance in a Magnetic Topological Insulator, Phys. Rev. Lett. **117**, 127202 (2016).

[28] Y. Fan, Q. Shao, L. Pan, X. Che, Q. He, G. Yin, C. Zheng, G. Yu, T. Nie, M. R. Masir, A. H. MacDonald, and K. L. Wang, Unidirectional magneto-resistance in modulation-doped magnetic topological insulators, Nano Lett. **19**, 692 (2019).

[29] K. Narayanapillai, K. Gopinadhan, X. Qiu, A. Annadi, Ariando, T. Venkatesan, and H. Yang, Current-driven spin orbit field in LaAlO$_3$/SrTiO$_3$ heterostructures, Appl. Phys. Lett. **105**, 162405 (2014).

[30] P. He, S. M. Walker, S. S.-L. Zhang, F. Y. Bruno, M. S. Bahramy, J. M. Lee, R. Ramaswamy, K. Cai, O. Heinonen, G. Vignale, F. Baumberger, and H. Yang, Observation of Out-of-Plane Spin Texture in a SrTiO$_3$ (111) Two-Dimensional Electron Gas, Phys. Rev. Lett. **120**, 266802 (2018).

[31] T. Guillet, C. Zucchetti, Q. Barbedienne, A. Marty, G. Isella, L. Cagnon, C. Vergnaud, H. Jaffrès, N. Reyren, J.-M. George, A. Fert, and M. Jamet, Observation of Large Unidirectional Rashba Magnetoresistance in Ge(111), Phys. Rev. Lett. **124**, 027201 (2020).

[32] H. Fangohr, D. S. Chernyshenko, M. Franchin, T. Fischbacher, and G. Meier, Joule heating in nanowires, Phys. Rev. B **84**, 054437 (2011).

[33] C. O. Avci, K. Garello, M. Gabureac, A. Ghosh, A. Fuhrer, S. F. Alvarado, and P. Gambardella, Interplay of spin-orbit torque and thermoelectric effects in ferromagnet/normal-metal bilayers, Phys. Rev. B **90**, 224427 (2014).

[34] T. Kikkawa, K. Uchida, S. Daimon, Y. Shiomi, H. Adachi, Z. Qiu, D. Hou, X.-F. Jin, S. Maekawa, and E. Saitoh, Separation of longitudinal spin Seebeck effect from anomalous Nernst effect: Determination of origin of transverse thermoelectric voltage in metal/insulator junctions, Phys. Rev. B **88**, 214403 (2013).

[35] M. Schreier, N. Roschewsky, E. Dobler, S. Meyer, H. Huebl, R. Gross, and S. T. Goennenwein, Current heating induced spin Seebeck effect, Appl. Phys. Lett. **103**, 242404 (2013).

[36] See Supplemental Material at http://link.aps.org/supplemental/10.1103/PhysRevMaterials.6.064201 for detail on experimental procedures, magnetic characterization, crystal structure, simulation parameters, temperature dependence of the UMR ratio, and substrate influence on the UMR ratio, which includes Refs. [44–51].

[37] T. Sato, S. Kokado, S. Kosaka, T. Ishikawa, T. Ogawa, and M. Tsunoda, Large negative anisotropic magnetoresistance in Co$_2$MnGa Heusler alloy epitaxial thin films, Appl. Phys. Lett. **113**, 112407 (2018).

[38] Y. Li, Y. Li, P. Li, B. Fang, X. Yang, Y. Wen, D.-x. Zheng, C.-h. Zhang, X. He, A. Manchon, Z.-H. Cheng, and X.-x. Zhang, Nonreciprocal charge transport up to room temperature in bulk Rashba semiconductor α-GeTe, Nat. Commun. **12**, 540 (2021).

[39] D. T. Son and B. Z. Spivak, Chiral anomaly and classical negative magnetoresistance of Weyl metals, Phys. Rev. B **88**, 104412 (2013).

[40] S. Tong, X. Zhao, D. Wei, and J. Zhao, Low-temperature resistivity anomaly and weak spin disorder in Co$_2$MnGa epitaxial thin films, Phys. Rev. B **101**, 184434 (2020).

[41] J. Gooth, F. Menges, N. Kumar, V. Süß, C. Shekhar, Y. Sun, U. Drechsler, R. Zierold, C. Felser, and B. Gotsmann, Thermal and electrical signatures of a hydrodynamic electron fluid in tungsten diphosphide, Nat. Commun. **9**, 4093 (2018).

[42] H. Ido and S. Yasuda, Magnetic properties of Co-Heusler and related mixed alloys, J. Phys. Colloq. **49**, C8-141 (1988).

[43] P. Brown, K.-U. Neumann, P. Webster, and K. Ziebeck, The magnetization distributions in some Heusler alloys proposed as half-metallic ferromagnets, J. Phys.: Condens. Matter **12**, 1827 (2000).

[44] E. C. Stoner and E. Wohlfarth, A mechanism of magnetic hysteresis in heterogeneous alloys, Philos. Trans. R. Soc. London A **240**, 599 (1948).

[45] N. Nagaosa, J. Sinova, S. Onoda, A. H. MacDonald, and N. P. Ong, Anomalous Hall effect, Rev. Mod. Phys. **82**, 1539 (2010).

[46] C. R. Akouala, R. Kumar, S. Punugupati, C. L. Reynolds, J. G. Reynolds, E. J. Mily, J.-P. Maria, J. Narayan, and F. Hunte, Planar Hall effect and anisotropic magnetoresistance in semiconducting and conducting oxide thin films., Appl. Phys. A **125**, 293 (2019).

[47] K.-I. Uchida, Transport phenomena in spin caloritronics, Proc. Jpn. Acad., Ser. B **97**, 69 (2021).

[48] Y. Pu, E. Johnston-Halperin, D. D. Awschalom, and J. Shi, Anisotropic Thermopower and Planar Nernst Effect in Ga$_{1-x}$Mn$_x$As Ferromagnetic Semiconductors, Phys. Rev. Lett. **97**, 036601 (2006).

[49] M. Saidi and R. H. Abardeh, Air pressure dependence of natural-convection heat transfer, in *Proceedings of the World Congress on Engineering* (WCE 2010 London, UK, 2010), Vol. 2, p. 1444.

[50] J. S. Arthur, The specific heats of MgO, TiO$_2$, and ZrO$_2$ at high temperatures, J. Appl. Phys. **21**, 732 (1950).

[51] A. J. Slifka, B. J. Filla, and J. Phelps, Thermal conductivity of magnesium oxide from absolute, steady-state measurements, J. Res. Natl. Inst. Stand. Technol. **103**, 357 (1998).